SENSITIVITY ANALYSIS OF SEMI-ANALYTICAL MODELS OF DIFFUSE ATTENTUATION OF DOWNWELLING IRRADIANCE IN LAKE BALATON

Van der Zande D.[1], Blaas M.[2], Nechad B.[1]

[1]*Royal Belgian Institute of Natural Sciences (RBINS),Gulledelle 100, B-1200 Brussels, Belgium,*
Email: d.vanderzande@naturalsciences.be
[2]*Deltares, Boussinesqweg 1, 2629 HV Delft, The Netherlands , Email:meinte.blaas@deltares.nl*

ABSTRACT

A quantification of the available light in the water column is key to evaluate the water quality in lakes as it is one of the major factors determining primary production. The light environment in water is generally described in terms of the vertical attenuation coefficient (Kd) and euphotic depth (Ze) where the light is reduced to 1% of its (just below) surface value. Reliable models to estimate KdPAR (and Ze) from remote sensing measurements have been successfully demonstrated in marine applications using typical ocean colour missions such as MERIS-envisat (300m) and MODIS-AQUA (250-1000m). In this study, we present the adaptation of a semi-analytical model for Kd and Ze, developed for MERIS/MODIS, to the new and upcoming sensors bands for inland water cases.

1. Introduction

The current and upcoming sensors such as Landsat-8 OLI, Sentinel-2 MSI and Sentinel-3 OLCI hold great potential to deliver new and improved products for inland water quality monitoring. To evaluate the water quality in lakes, ecosystem modelers require information on the available light in the water column as it is one of the major factors determining primary production. This light environment is generally described in terms of the available Photosynthetically Available Radiation (PAR) in the water column, the PAR vertical attenuation coefficient (KdPAR) and the euphotic depth (Ze) where PAR is reduced to 1% of its (just below) surface value. Reliable models to estimate KdPAR (and Ze) from remote sensing measurements have been successfully demonstrated in marine applications using typical ocean colour missions such as MERIS-Envisat (300m) and MODIS-AQUA (250-1000m). Remote sensing reflectance (Rrs) can be used to determine Kd and Ze with empirical relationships between Kd and ratios (or values) of irradiance reflectance. The first algorithms were set up as part of the inverse problem, thus giving Kd as a function of the blue-to-green ratio of Rrs (Austin and Petzold, 1980; Gould and Arnone, 1994; Mueller and Trees, 1997; Loisel et al., 2001). In two-step algorithms, Kd is related to water constituents which are retrieved from Rrs (Morel, 1988; Morel et al., 2007). Generally, these types of algorithms are simple and require a minimal amount of processing power but they often only apply to the type of waters from which they were developed. Alternatively, the multiband quasi-analytical algorithm (QAA) (Lee et al, 2002) was developed to derive absorption and backscattering coefficients by inverting spectral Rrs(λ). The absorption and backscatter coefficients are subsequently used to estimate Kd (Lee et al. 2005a; Lee et al., 2005b, Lee et al., 2007). QAA has been successfully demonstrated in marine applications using typical ocean colour missions such as MERIS-Envisat (300m) and MODIS-AQUA (250-1000m).

In this study, we explore the adaptation of a semi-analytical model for Kd and Ze, developed for the MERIS/MODIS sensors and marine water types, to the new and upcoming sensors bands (i.e. L8, S2 and S3) for inland water cases. The adaptation of the model is based on the investigation of the impact of differences in the spectral response functions of the considered sensors on the models accuracy.

2. Materials and Methods

2.1. Rrs spectra and Signal Response Functions

In this study the IOCCG synthetic data set, simulated using the widely accepted numerical code HydroLight (Mobley, 1995), was used. This dataset contains a total of 500 points with both inherent (IOP) and apparent (AOP) optical properties. The IOPs (i.e. absorption and backscattering coefficients) were generated with various available optical/bio-optical parameters/models, while AOPs (remote sensing reflectance Rrs, Kd) were generated using Hydrolight with the available IOPs (see figure 1). It is important to state here that the IOPs represent marine water types with chlorophyll a concentrations ranging from 0.03µg/l to 30 µg/l in 20 steps. For each step the absorption coefficients of detritus/minerals and Colour Dissolved Organic Matter (CDOM) are varied randomly within set constraints. This results in a comprehensive data set used for algorithm development and testing with IOP and AOP values per 10nm in a spectral range of 400nm to 800nm. For more details see IOCCG report 5.

The Rrs values of this dataset were subsequently subsampled using the Spectral Response Functions

(SRF, figure 2) of the L8-OLI and S2-MSI to simulate L8 and S2 datasets (Barsi et al, 2014) for the relevant bands (i.e. 443nm, 490nm, 560nm, 665nm for S2-MSI and 655nm for L8-OLI). No signal-to-noise ratios were taken into account when generating the L8-OLI and S2-MSI datasets. More details of the band characteristics of the considered sensors can be found in table 1.
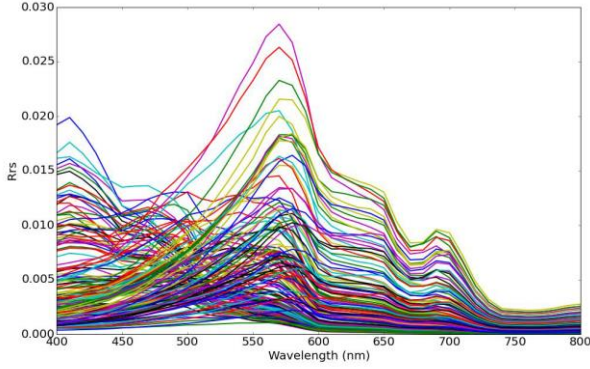
Figure 1.Rrs spectra of moderate case 1 water types simulated using Hydrolight

Characteristics of spectral band set of considered sensors are presented in table 1. The IOCCG dataset was not resampled for the L3-OLCI sensor as its bandwidths are approximately 10 nm, similar to the IOCCG dataset. As the SRF of S3-OLCI are quasi rectangular, the IOCCG dataset is considered as an adequate representation of the S3-OLCI bands and will be used as reference for further processing.

Table 1: Characteristics of spectral band set of considered sensors

central wavelength	S3-OLCI bandwidth	S2-MSI bandwidth	L8-OLI bandwidth
443nm	10nm	20 nm	16 nm
490nm	10 nm	65 nm	60 nm
560nm	10 nm	35 nm	57 nm
655nm	x	x	37 nm
665nm	10 nm	30 nm	x
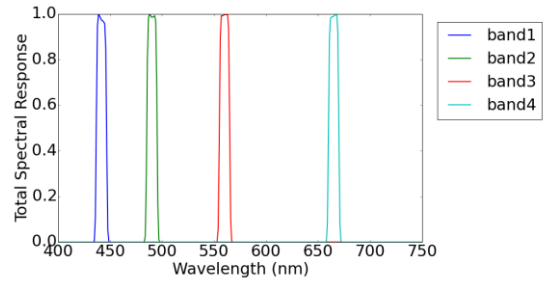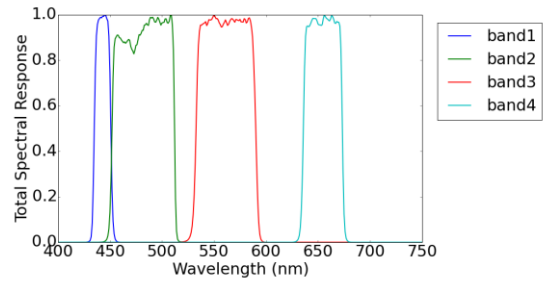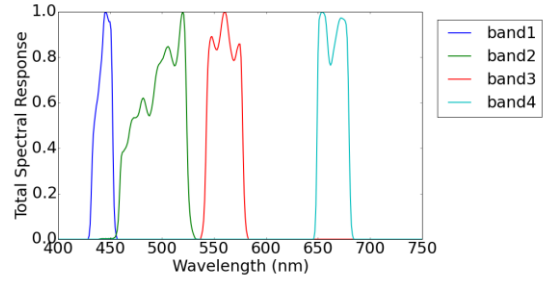
Figure 2.Spectral Response function of the S2-MSI (top), L8-OLI (middle) and S3-OLCI (bottom) sensors for bands relevant to this study

2.2. Quasi-analytical algorithm (QAA) for Kd

The multi-band QAA is developed to retrieve absorption (a) and backscattering (bb) coefficients for open and coastal waters from Rrs measurements. In a next step a and bb can be used to determine Kd and Ze. The algorithm was originally designed for data from MERIS and MODIS but can be applied to current and future sensors. The basic algorithm consists of five steps to calculate the total a and bb from Rrs data for a chosen band. Two of these steps are based on empirical relationships which are tested in this study for use with data from sensors L8-OLI and S2-MSI which are originally developed for land applications. The IOCCG dataset provides reference material for each of the QAA

steps enabling a direct calibration of the QAA to data from the new sensors. All Rrs datasets (i.e. S3-reference, S2, and L8) are used as input for the model and the output is compared to the reference data.

Step 0 & 1 $r_{rs}(\lambda)$ $\upsilon(\lambda)=f(r_{rs}(\lambda))$

$Y=f(r_{rs}(443),r_{rs}(560))$

Step 2 $a(\lambda_0) = a_w(\lambda_0) + f(r_{rs}443, r_{rs}490, r_{rs}665)$

Step 3 $b_{bp}(\lambda_0) = f(\upsilon(\lambda_0), a(\lambda_0), b_{bw}(\lambda_0))$

Step 4 $b_{bp}(\lambda) = b_{bp}(\lambda_0)(\lambda_0/\lambda)^Y$

Step 5 $a(\lambda) = f(\upsilon(\lambda_0), b_{bp}(\lambda_0), b_{bw}(\lambda_0))$

Step Kd $Kd(\lambda) = m_0 a + m_1(1-m_2 e^{-m_3 a}) b_b$
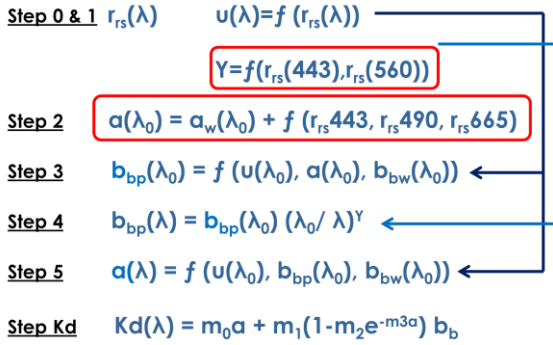
Figure 3.Different steps of the QAA to calculate kd from Rrs with the empirical steps highlighted in red. These steps are sensitive to the larger bandwidths of the S2-MSI and L8-OLI sensors

3. Results and Discussion

3.1. Simulated S2 and L8 Rrs observations

In the QAA it is necessary to first invert the reflectance signal to provide a and bb coefficients which are then used to determine the spectral Kd. While the central wavelength of the relevant bands do not differ greatly between the considered sensors, the SRFs show significant differences between the ocean colour sensor (S3-OLCI) and the land sensors (S2-MSI and L8-OLI) as can be observed in figure 2. The squared shaped bands of S3-OLCI are narrow (approx. 10nm) resulting in accurate measurements of the central wavelength. The bands of the land sensors are wider and irregular shaped which results in differences in the measured spectral reflection compared to a narrow band system like S3-OLCI. Figure 4 shows a direct comparison between simulated S2-MSI and L8-OLI and the IOCCG dataset which is considered to be representative of the S3-OLCI sensor. The 443nm band is slightly underestimated for both S2-MSI and L8-OLI bands (6.52% and 4.95% respectively) compared to S3-OLCI. The 490nm band for S2_MSI underestimates Rrs for 9.98% and introduces more scatter caused by the wider bandwidth and irregular shaped SRF. The L8-OLI 490nm band results in an underestimation of 4.73% but no increased scatter was observed, even with the larger bandwidth. This could be explained by the fact that the SRF for the 490nm band is not as irregular compared to the SE-MSI SRF. The 560nm bands of S2-MSI and L8-OLI underestimate the Rrs by 1.10% and 3.87% respectively. For both bands more scatter is introduced which is expected to be a result of a combination of the increased bandwidth, SRF shapes and Rrs spectra shapes.
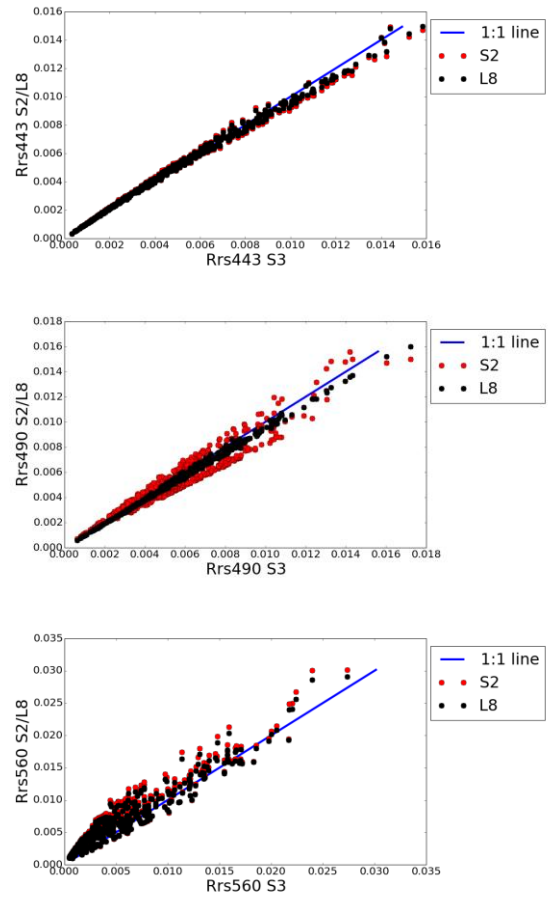
Figure 4. Direct comparison of Rrs values between the S3-OLCI and S2-MSI/L8-OLI sensors for the spectral bands: 443nm (top), 490nm (middle) and 560nm (bottom)

Due to a lack of a 655nm band for S3-OLCI the simulated Rrs values for L8-OLI were compared to the reference data for that specific band from the IOCCG dataset. Figure 5 shows that the Rrs values for L8-OLI are 2.44% lower that the IOCGG reference values. A direct comparison between S3-OLCI and S2-MSI for the 665nm band showed an overestimation of 8.60%. While the same IOCCG data set was used to generate the simulated datasets for the three considered sensors, the results show that the resulting Rrs values show differences due to the bandwidth, SRF shapes and Rrs spectra shapes of the different sensors. In the next step we will investigate how these differences propagate through the QAA and eventually influence the final products, the Kd and Ze.

3.2. a and bb coefficients from QAA

Figure 6 shows the $a(\lambda_0)$ and $bb(\lambda_0)$ calculated using equations (1) and (4) for each sensor compared to the
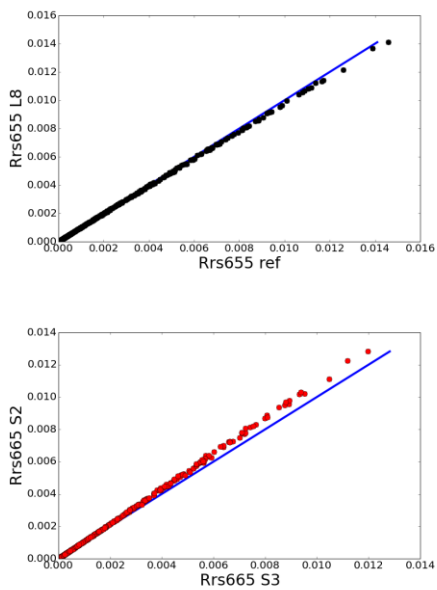
Figure 5. Direct comparison of Rrs values between the IOCCG dataset and the L8-OLI 655nm band (top) and between the S3-OLCI and S2-MSI sensors for the 665nm band and(bottom).

reference values available in the IOCCG dataset. These coefficients are subsequently used to calculate the spectral coefficients $a(\lambda)$ and $bbp(\lambda)$ The blue, red and black dots represent the results for S3-OLCI, S2-MSI and L8-OLI respectively. While the derived $a(670)$ does not yield good results, these properties are of second order importance, i.e. its inaccuracy does not significantly affect the end results. The $a(670)$ values for S3-OLCI follow the 1:1 relationship (slope=0.99, r^2=0.78). The impact of the bandwidth and SRF is noticeable as the slope for the $a(670)$ comparison deviates more for the land sensors: 1.06 (r^2=0.80) for S2-MSI and 1.35 (r^2=0.80) for L8-OLI. The estimation of $bbp(670)$ yields better results for S3-OLCI (slope=1.04, r^2=0.95). For the land sensors we see an increase in the slope: 1.26 (r^2=0.96) for S2_MSI and 1.55 (r^2=0.95) for L8. The comparison of the Rrs values of the relevant bands (figure 4 and 5) showed that the difference in bandwidth and SRF shapes between ocean colour and land sensors resulted in changes in the linear relationships as well as more variability in the land sensor measurements. When propagated through the QAA, these differences in Rrs resulted in a different slope but with no more variability in the resulting $a(\lambda_0)$ and $bb(\lambda_0)$ estimates. This means that correction factors can be determined from the difference in slopes in the $a(670)$ and $bbp(670)$ relationships to bring the accuracy of the estimation of the mentioned coefficients for the land sensors to the same level as the ocean colour sensors.
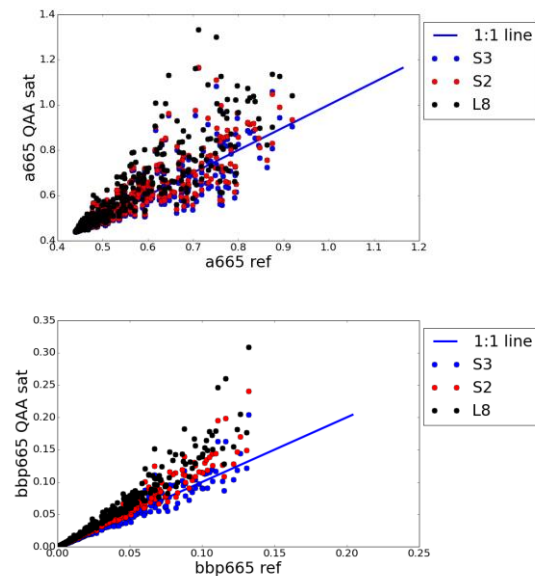
Figure 6. Estimated bbp at 665nm versus reference bbp values (x-axis) as available in the IOCCG dataset (top).Estimated a at 665nm versus reference a values (x-axis) as available in the IOCCG dataset (bottom)

3.3. Spectral Kd

Spectral Kd is estimated based on coefficients $a(\lambda)$ and $bbp(\lambda)$ as calculated by the QAA. Figure 7 shows $Kd(\lambda)$ for each sensor compared to the reference values available in the IOCCG dataset. The blue, red and black dots represent the results for S3-OLCI, S2-MSI and L8-OLI respectively. For $Kd(443)$ covering a range of 0.02-4.1m^{-1}, the mean absolute percentage errors (MAPE) are 9.28%, 13.58% and 28.92% for S3-OLCI, S2-MSI and L8-OLI respectively. Linear regression slopes are 1.16 (r^2=0.95), 1.29 (r^2=0.97) and 1.59 (r^2=0.96) for S3-OLCI, S2-MSI and L8-OLI respectively. For lower $Kd(443)$ values ($Kd(443 < 2.5m^{-1})$ the QAA performs well using the S3-OLCI dataset but at the high end, $Kd(443)$ is overestimated. For land sensors, the MAPE increases as a direct result of an increase of slope with a minimal decrease of the fit of the linear regression (r^2=95-97). Similar patterns are observed for $Kd(490)$ and $Kd(560)$. While MAPE values for $Kd(655)$ are lower at lower wavelengths, the overall variability is higher.
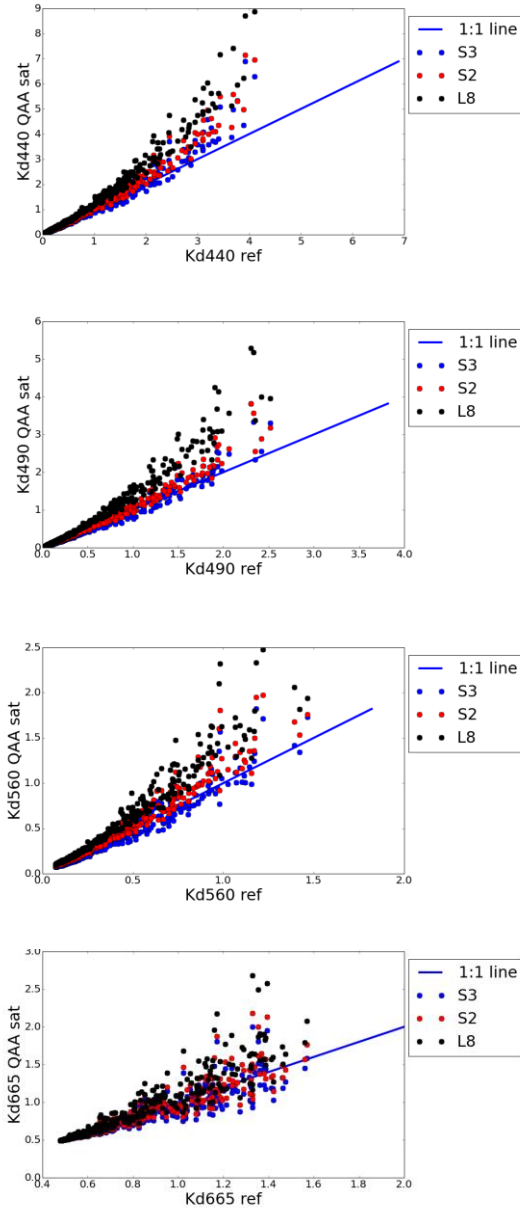
Figure 7. QAA-derived Kd(λ) (i.e. Rrs-derived) versus the Kd from the IOCCG dataset.

Table 2 presents statistical parameters describing the direct comparison between QAA-derived Kd estimates and reference values. Based on the IOCCG dataset, the slope of linear regression is suggested as the first parameter of the correction factor to adapt the QAA-based Kd estimates to bandsets of S2-MSI and L8-OLI.

Table 2. Statistical parameters describing the direct comparison between QAA-derived Kd estimates and reference values. Based on the IOCCG dataset, the slope of linear regression is suggested as the correction factor to adapt the QAA-based Kd estimates to bandsets of S2-MSI and L8-OLI.

| | S3-OLCI | | | S2-MSI | | | L8-OLI | | |
	MAPE	slope	R^2	MAPE	slope	R^2	MAPE	slope	R^2
Kd(443)	9.28	1.16	0.95	13.58	1.29	0.97	28.90	1.59	0.96
Kd(490)	9.63	1.09	0.95	14.92	1.18	0.97	31.38	1.63	0.96
Kd(560)	10.35	1.04	0.95	11.56	1.21	0.96	30.53	1.48	0.95
Kd(665)	5.52	0.92	0.87	5.09	1.06	0.87	7.63	1.31	0.88

4. Conclusions

QAA is a semi-analytical algorithm based on solutions of the radiative transfer equation which can be applied to different water types, and retrieval accuracy is often much better that a straight-forward empirical algorithm. To limit time-consuming computations, different steps in the QAA are based on empirical relationships. These relationships were calibrated using data obtained in marine waters (i.e. case 1 and coastal waters) for use with narrow band sensors such as MERIS and MODIS. With this study we assessed the impact of the broader bandwidths of the S2-MSI and L8-OLI sensors on the different steps of the QAA. First results showed that in terms of spectral Kd estimates, small increases in errors (e.g. MAPE) could be observed for the S2-MSI sensor for the blue and green bands. In the case of L8-OLI these errors were bigger (MAPE > 28%) which we assume to be a results of the more irregular shaped SRFs. While these errors in Kd estimation increased for the land sensors, the regression coefficients did not as the comparison between QAA-based spectral Kd and reference values resulted in a shift in the slope of the linear regression. This shift can easily be used as a correction factor for Kd when using data from the land sensors making for inland water applications.

With Hydrolight we are able to expand the synthetic data set to extreme turbid or eutrophic conditions which can be present in inland water. This will enable us in the future to investigate the sensitivity of the QAA in these conditions. First results indicate that the sensitivity of the QAA decreases in extremely turbid conditions (TSM > 100mg/l) and that an additional adaptation of the QAA is needed for all sensors including L8-OLI, S2-MSI and S3-OLCI. Subsequently, the adapted model for KdPAR will be implemented in the numerical water quality and biogeochemical model Delft3D WAQ (e.g., Los et al., 2008) to investigate the interaction of the optical properties with the primary production.

References

Austin, R.W., and Petzold, T. (1981) The determination of the diffuse attenuation coefficient of sea water using the Coastal Zone Color Scanner. Oceanography from Space, J.F.R. Gower, Ed., Plenum Press, 239–256

Barsi J., Lee K., Kvaran G., Markham B., Pedelty J. (2014). The Spectral Response of the Landsat-8 Operational Land Imager. *Remote Sens,*, 6, 10232-10251

Gould R., Arnone R. (1994), Extending Coastal Zone Color Scanner estimates of the diffuse attenuation coefficient into Case II waters, Proc. SPIE 2258, Ocean Optics XII, 342 (October 26, 1994)

IOCCG (2006). Remote Sensing of Inherent Optical Properties: Fundamentals, Tests of Algorithms, and Applications. Lee, Z.-P. (ed.), Reports of the International Ocean-Colour Coordinating Group, No. 5, IOCCG, Dartmouth, Canada.

Lee Z., Kendall L., Arnone R. (2002) Deriving inherent optical properties from water color: a multiband quasi-analytical algorithm for optically deep waters. Applied Optics, 41(27), 5755-5772

Lee, Z., A. Weidemann, et al. (2007). "Euphotic zone depth: its derivation and implication to ocean-color remote sensing." Journal of Geophysical Research 112 C03009)

Lee, Z., K. Du, et al. (2005). "A model for the diffuse attenuation coefficient of downwelling irradiance." Journal of Geophysical Research 110(C02016).

Lee, Z., M. Darecki, et al. (2005). "Diffuse attenuation coefficient of downwelling irradiance: an evaluation of remote sensing methods." Journal of Geophysical Research 110(C02107).

Los, F.J., M.T. Villars, M.W.M. Van der Tol, (2008) A 3-dimensional primary production model (BLOOM/GEM) and its applications to the (southern) North Sea (coupled physical–chemical–ecological model), Journal of Marine Systems, Volume 74, Issues 1–2, Pages 259-294

Morel A. (1988) Optical modelling of the upper ocean in relation to its biogenous matter content (Case I waters). Journal of Geophysical Research, 93, 10749-10768.

Morel A., Antoine, D., Gentili, B. (2007) Natural variabililty of bio-optical properties in Case 1 waters: attenuation and reflectance within the visible and near-UV spectral domains, as observed in South Pacific and Mediterraneean waters. Biogeosciences, 4, 913-925.

Mueller, J., Trees C., (1997), Revised SeaWiFS prelaunch algorithm for the diffuse attenuation coefficient K(490). In: Yeh, E-n., R.A. Barnes, M. Darzi,